NAIC-ID(RS)T-0410-96

NATIONAL AIR INTELLIGENCE CENTER

SELECTED ARTICLES

**Approved for public release:
distribution unlimited**

HUMAN TRANSLATION

NAIC-ID(RS)T-0410-96 9 October 1996

MICROFICHE NR:

SELECTED ARTICLES

English pages: 22

Source: Journal of Astronautics, Vol. 16, Nr. 4, 1995
(Cama, Vol. 3, Nr. 1, 1996); pp. 9-15; 80-84

Country of origin: China
Translated by: Leo Kanner Associates
F33657-88-D-2188
Requester: NAIC/TASC/Richard A. Peden, Jr.
Approved for public release: distribution unlimited.

TABLE OF CONTENTS

GRAPHICS DISCLAIMER

All figures, graphics, tables, equations, etc. merged into this translation were extracted from the best quality copy available.

Research on Minimum-Fuel Fixed Thrust Transfers Between Coplanar Orbits

Wang Xiaojun, Wu Delong, Yu Menglun

(Beijing Aeronautics System Engineering Research Institute, Beijing, 100076)

Abstract: This paper studies a minimum-fuel thrust direction control strategy for a primary insertion from a circular (or elliptical) orbit to a coplanar (or elliptical) orbit with a fixed thrust. Problems of this kind can be incorporated into the double-bound value problem, which is discussed with reference to the selection of initial free values and the burn method is used for an iterative solution. Also in this paper, optimal transfer from a parking orbit to a geosynchronous transfer orbit, and between two near-earth circular orbits are calculated, with satisfactory results.

Key words: orbit transfer, minimum fuel consumption, principle of the maximum, optimal control

1. Introduction

Spacecraft are generally required to accomplish one or several dynamic orbit transfers before entering a target orbit and therefore it is vitally important to design an orbit transfer process which spares propellant and reduces the spacecraft mass. The conventional design of orbit transfer is based on the Hohmann optimal orbit transfer theory under the fundamental assumption that velocity variation is completed in an instant, i.e. an impulsive orbit transfer. This is fairly accurate with a larger thrust. However, given the diversification of flight missions, the requirements for overload becomes more and more rigorous and the amount of thrust is restricted. Under such a scenario, more and more attention has been given to limited or small thrust multiple orbit transfers during extended upper level space flight missions or interstellar probes [1]. When propelled with a small thrust, a spacecraft must fly dynamically long distances in space

and may suffer from velocity losses caused by gravity. In this case, a major concern is how to control the variation of the thrust vector so as to reduce the velocity losses and much research has been done on this aspect [2,3].

The variational method and the principle of the maximum are effective methods to solve, respectively, the problem of liberating control of constraints and the problem of optimizing the control constraints. An analytical solution can be obtained for a simple situation, yet a complex multivariable problem such as space track optimization requires an iterative solution of double-bound values [3-7]. The major difficulty in this solution is how to select the initial values of those conjugate variables that are not physically meaningful, while the equation is extremely nonlinear and its convergence depends on the accurate selection of the initial values [3,5,7]. Thus, it is very important to transform the initial free values into physically meaningful variables and adopt some efficient measures in calculations based on the possible optimal results.

In this paper the authors derive the optimal process and analyze in detail the bound-value conditions for various initial orbits and target orbits based on the different characteristics of circular orbits and elliptical orbits. Also discussed is how to select initial free-value variables using the initial integration descending order. Finally the calculations are carried out for the fixed thrust optimal transfer from a parking orbit to a geosynchronous transfer orbit, and between two circular orbits, together with an analysis of the optimal results.

2. Theoretical Analysis

By using a reference radius r_{ref}, reference time (g_{ref} is gravitational acceleration at r_{ref}) and initial mass m_0 to make the equation non-dimensional, a non-dimensional dynamic

equation in the inverse ratio squared gravitational field can be derived [2]:

$$\begin{aligned}
\frac{dr}{d\tau} &= V\sin\gamma \\
\frac{d\theta}{d\tau} &= \frac{V\cos\gamma}{r} \\
\frac{dV}{d\tau} &= -\frac{\sin\gamma}{r^2} + G\frac{\cos\alpha}{m} \\
\frac{d\gamma}{d\tau} &= \left(\frac{V^2}{r} - \frac{1}{r^2}\right)\frac{\cos\gamma}{V} + G\frac{\sin\alpha}{mV} \\
\frac{dm}{d\tau} &= -G\frac{1}{V_e}
\end{aligned} \tag{1}$$

where r, θ, V, γ, m, respectively, are the geocentric distance, polar angle, velocity, flight track angle and mass, which are referred to as state variables; V_e is the engine gas injection speed which is taken as a constant; $G=T/m_0 g_{ref}$, T is engine thrust; Earth's radius is usually selected as r_{ref}, then G is the initial thrust-weight ratio; α is the angle of attack.

The goal of optimization is minimum fuel consumption m_p, which is equivalent to the maximum orbital insertion mass $m(\tau_f)$; the angle of attack α is a control parameter to be optimized.

By introducing the Hamiltonian function in Eq. (1):

$$\begin{aligned}
H = {} & \lambda_r V\sin\gamma + \lambda_\theta\frac{V\cos\gamma}{r} + \lambda_V\left(-\frac{\sin\gamma}{r^2} + G\frac{\cos\alpha}{m}\right) \\
& + \lambda_\gamma\left[\left(\frac{V^2}{r} - \frac{1}{r^2}\right)\frac{\cos\gamma}{V} + G\frac{\sin\alpha}{mV}\right] - \lambda_m G\frac{1}{V_e}
\end{aligned} \tag{2}$$

λ_r、λ_θ、λ_V、λ_γ、λ_m are the conjugate variables corresponding to the state variables, which must obey the following differential equation along the optimal flight track in accordance with the optimization theory [2]:

$$\begin{aligned}
\frac{d\lambda_r}{d\tau} &= \lambda_\theta\frac{V\cos\gamma}{r^2} + \lambda_\gamma\left(\frac{V^2}{r^2} - \frac{2}{r^3}\right)\frac{\cos\gamma}{V} - \lambda_V\frac{2\sin\gamma}{r^3} \\
\frac{d\lambda_\theta}{d\tau} &= 0 \\
\frac{d\lambda_V}{d\tau} &= -\lambda_r\sin\gamma - \lambda_\theta\frac{\cos\gamma}{r} - \lambda_\gamma\left[\left(\frac{1}{r} + \frac{1}{r^2V^2}\right)\cos\gamma - \frac{G\sin\alpha}{mV^2}\right] \\
\frac{d\lambda_\gamma}{d\tau} &= -\lambda_r V\cos\gamma + \lambda_\theta\frac{V}{r}\sin\gamma + \lambda_V\frac{1}{r^2}\cos\gamma + \lambda_\gamma\left(\frac{V^2}{r} - \frac{1}{r^2}\right)\frac{\sin\gamma}{V}
\end{aligned} \tag{3}$$

$$\frac{d\lambda_m}{d\tau} = \frac{G}{m^2}\left(\lambda_V \cos\alpha + \lambda_\gamma \frac{\sin\alpha}{V}\right) \tag{3}$$

From the optimal principle:

$$\frac{\partial H}{\partial \alpha} = -\lambda_V G \frac{\sin\alpha}{m} + \lambda_\gamma G \frac{\cos\alpha}{mV} = 0$$

is derived:

$$\alpha = \tan^{-1} \frac{\lambda_\gamma}{\lambda_V V} \tag{4}$$

The Hamiltonian function H does not contain distinct time τ and is an autonomous system [2]; the terminal time τ_f is free and the performance index and terminal constraint do not contain distinct τ_f. Therefore:

$$H(\tau_0) = H(\tau) = H(\tau_f) = 0 \tag{5}$$

From Eq. (3) $\frac{d\lambda_\theta}{d\tau} = 0$, (6)

$$\lambda_\theta(\tau) = C_1$$

Based on Eqs. (1), (3) and (4), if the initial values of state variables and conjugate variables are known, the solution to the problem can be derived through numerical integration.

3. Analysis of Bound Value Conditions

The orbital constraint mode is given by orbit parameters, including eccentricity e, energy ζ and argument of perigee ω. Their relationship with state variables is [2]:

$$e = \sqrt{1 + \upsilon(\upsilon - 2)\cos^2\gamma}, \quad \zeta = \frac{V^2}{2} - \frac{1}{r}, \quad \omega = \theta - \tan^{-1}\frac{p\tan\gamma}{p - r}$$

where $p = r^2V^2\cos^2\gamma$, $\upsilon = rV^2$

With different initial orbits and target orbits, the corresponding bound value problems are also different.

3.1 The Case When the Target Orbit is an Elliptical Orbit

The parameters of target orbit are e_f, ζ_f, ω_f. The state variables should satisfy the constraint equation in the terminal time as follows:

$$\begin{cases} \Psi_1(\tau_f) = \sqrt{1 + \upsilon(\tau_f)(\upsilon(\tau_f) - 2)\cos^2\gamma(\tau_f)} - e_f = 0 \\ \Psi_2(\tau_f) = \frac{1}{2}V^2(\tau_f) - \frac{1}{r(\tau_f)} - \zeta_f = 0 \\ \Psi_2(\tau_f) = \theta(\tau_f) - \tan^{-1}\frac{p(\tau_f)\tan\gamma(\tau_f)}{p(\tau_f) - r(\tau_f)} - \omega_f = 0 \end{cases} \tag{7}$$

then the terminal transverse conditions are:

$$\lambda_r(\tau_f) = \upsilon_1\frac{\partial\Psi_1}{\partial r(\tau_f)} + \upsilon_2\frac{\partial\Psi_2}{\partial r(\tau_f)} + \upsilon_3\frac{\partial\Psi_3}{\partial r(\tau_f)}, \qquad \lambda_\theta(\tau_f) = \upsilon_3$$

$$\lambda_V(\tau_f) = \upsilon_1\frac{\partial\Psi_1}{\partial V(\tau_f)} + \upsilon_2\frac{\partial\Psi_2}{\partial V(\tau_f)} + \upsilon_3\frac{\partial\Psi_3}{\partial V(\tau_f)}, \qquad \lambda_\gamma(\tau_f) = \upsilon_1\frac{\partial\Psi_1}{\partial\gamma(\tau_f)} + \upsilon_3\frac{\partial\Psi_3}{\partial\gamma(\tau_f)}$$

From the above, the following equation can be derived:

$$\lambda_r(\tau_f) - \frac{1}{r^2(\tau_f)V(\tau_f)}\lambda_V(\tau_f) + \frac{1}{r(\tau_f)\tan\gamma(\tau_f)}\lambda_\theta(\tau_f) + \frac{1}{r(\tau_f)\tan\gamma(\tau_f)}\left(1 - \frac{1}{r(\tau_f)V^2(\tau_f)}\right)\lambda_\gamma(\tau_f) = 0 \tag{8}$$

Eqs. (7) and (8) contain four constraining equations.

3.1.1 The Case When the Initial Orbit is an Elliptical Orbit

The orbit parameters are e_0, ζ_0, ω_0. If the orbital transfer location is not restricted, they should meet the following constraints in the initial time:

$$\begin{cases} \Phi_1(\tau_0) = \sqrt{1 + \upsilon(\tau_0)(\upsilon(\tau_0) - 2)\cos^2\gamma(\tau_0)} - e_0 = 0 \\ \Phi_2(\tau_0) = \frac{1}{2}V^2(\tau_0) - \frac{1}{r(\tau_0)} - \zeta_0 = 0 \\ \Phi_3(\tau_0) = \theta(\tau_0) - \tan^{-1}\frac{p(\tau_0)\tan\gamma(\tau_0)}{p(\tau_0) - r(\tau_0)} - \omega_0 = 0 \\ \Phi_4(\tau_0) = m(\tau_0) - 1 = 0 \end{cases} \tag{9}$$

The transverse conditions at the initial moment are:

$$\lambda_r(\tau_0) = \mu_1\frac{\partial\Phi_1}{\partial r(\tau_0)} + \mu_2\frac{\partial\Phi_2}{\partial r(\tau_0)} + \mu_3\frac{\partial\Phi_3}{\partial r(\tau_0)}, \quad \lambda_\theta(\tau_0) = \mu_3$$

$$\lambda_V(\tau_0) = \mu_1\frac{\partial\Phi_1}{\partial V(\tau_0)} + \mu_2\frac{\partial\Phi_2}{\partial V(\tau_0)} + \mu_3\frac{\partial\Phi_3}{\partial V(\tau_0)}$$

$$\lambda_\gamma(\tau_0) = \mu_1\frac{\partial\Phi_1}{\partial\gamma(\tau_0)} + \mu_3\frac{\partial\Phi_3}{\partial\gamma(\tau_0)}, \quad \lambda_m(\tau_0) = \mu_4$$

Then the relationship similar to Eq. (8) is derived as:

$$\begin{aligned} \lambda_\theta(\tau_0) = &- r(\tau_0)\tan\gamma(\tau_0)\lambda_r(\tau_0) + \frac{\tan\gamma(\tau_0)}{r(\tau_0)V(\tau_0)}\lambda_V(\tau_0) \\ &- \left[1 - \frac{1}{r(\tau_0)V^2(\tau_0)}\right]\lambda_\gamma(\tau_0) \end{aligned} \tag{10}$$

Since (3) differential equation of conjugate variables is linearly homogenous, the initial value of one conjugate variable can be determined randomly (with the required symbol) [4], which is taken as:

$$\lambda_m(\tau_0) = 1.0 \tag{11}$$

By substituting Eqs. (10) and (11) in (5) and forming simultaneous a set if equations with Eq. (4), then:

$$\lambda_\gamma(\tau_0) = \frac{V(\tau_0)}{V_e}\sin\alpha(\tau_0), \quad \lambda_V(\tau_0) = \frac{1}{V_e}\cos\alpha(\tau_0) \tag{12}$$

The four equations (9-12) contain eight equations and eleven unknown variables (including α), of which three variables cannot be determined, supposedly $\theta(\tau_0)$, $\alpha(\tau_0)$, $\lambda_r(\tau_0)$, referred to as initial free values. There are four constraining conditions at termination: one of them is the integration termination condition (shut-down condition), while the other three constraints correspond to the three initial free values, formulating a double-bound value problem.

3.1.2 The Case When the Initial Orbit is a Circular Orbit

The orbit parameter is ζ_0, then the constraint is:

$$\begin{cases} \Phi_1(\tau_0) = r(\tau_0) + \dfrac{1}{2\zeta_0} = 0, \quad \Phi_2(\tau_0) = V(\tau_0) - \sqrt{-2\zeta_0} = 0 \\ \Phi_3(\tau_0) = \gamma(\tau_0) = 0, \quad \Phi_4(\tau_0) = m(\tau_0) - 1 = 0 \end{cases} \tag{13}$$

and the transverse condition is:

$$\lambda_\theta(\tau_0) = 0 \tag{14}$$

Eqs. (11-14) contain a total of eight equations as above, and the free initial values are still $\theta(\tau_0)$, $\alpha(T_0)$ and $\lambda_r(T_0)$

3.2 The Case When the Target Orbit is a Circular Orbit

The orbit parameter is ζ_f, and terminal constraint is:

$$\Psi_1(\tau_f) = r(\tau_f) + \frac{1}{2\zeta_f} = 0, \ \Psi_2(\tau_f) = V(\tau_f) - \sqrt{-2\zeta_f} = 0, \ \Psi_3(\tau_f) = \gamma(\tau_f) = 0 \tag{15}$$

The transverse condition is: $\lambda_\theta(\tau_f) = 0$

From Eq. (6), $$\lambda_\theta(\tau) = 0, \quad \lambda_\theta(\tau_0) = 0 \tag{16}$$

For the case when the target orbit is a circular orbit,

there are only three constraint conditions in Eq. (15) at the termination.

3.2.1 The Case When the Initial Orbit is an Elliptical Orbit

The initial constraint equation totally conforms to Eq. (9). By substituting Eqs. (16) in (10):

$$\lambda_r(\tau_0) = \frac{-1}{r(\tau_0)\tan\gamma(\tau_0)}\left(1 - \frac{1}{r(\tau_0)V^2(\tau_0)}\right)\lambda_\gamma(\tau_0) + \frac{1}{r^2(\tau_0)V(\tau_0)}\lambda_V(\tau_0) \qquad (17)$$

Thus, (9), (11), (12), (16) and (17) contain nine equations and two initial free values selected as $\theta(\tau_0)$ and $\alpha(\tau_0)$.

3.2.2 The Case When the Initial Orbit is a Circular Orbit

When both the initial orbit and target orbit are circular orbits, the location θ has no effect on the evaluation of other variables at the initial point and termination and $\lambda_\theta(\tau)=0$. Thus, θ and λ_θ can be omitted with nine variables remaining; Eqs. (11), (12) and (13) contain seven equations with two initial free values selected as $\alpha(\tau_0)$ and $\lambda_r(\tau_0)$.

4. Sample Calculation and Analysis of the Result

Sample Calculation 1 Transfer from a parking orbit (a circular orbit 200km in height) to a synchronous transfer orbit (apogee h_a=35786km, perigee h_p=200km, $\omega=180^0$). V_e=4500m/s.

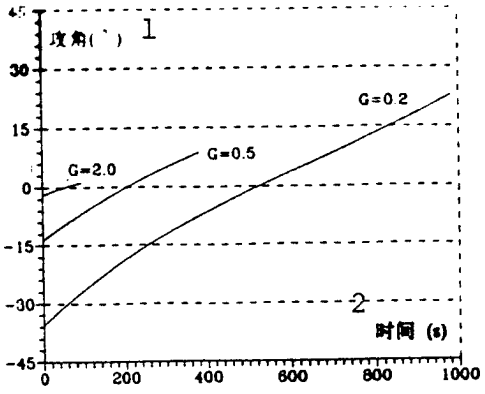

Fig. 1 Optimal Angle of Attack Variation Law

Key: (1) Angle of attack; (2) Time

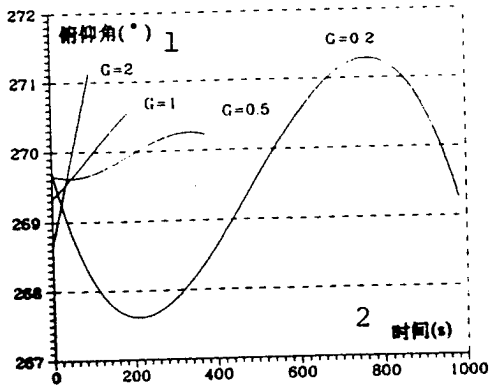

Fig. 2 Pitch Angle variation Law

Key: (1) Pitch angle; (2) Time

Figure 1 shows the optimal variation law of attack angle α, which is close to a linear variation with extremely large variation amplitude of α when the thrust is small. Fig. 2 displays the variation law of pitch angle $\varphi(t)$ in inertial space when G varies ($\varphi = \theta + 90° - \alpha - \gamma$); φ varies in a smaller amplitude despite the large variation of α with a small thrust. Generally speaking, $\varphi(t)$ is designed to be in a linear variation [8] in engineering. Obviously, with a small thrust, the number of segments should be increased so as to obtain an optimal control law.

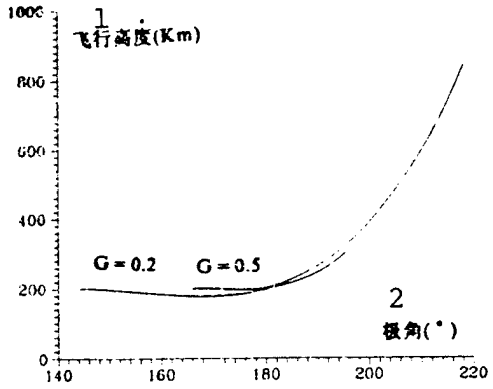

Fig. 3 Variation of Flight Altitude

Key: (1) Flight altitude; (2) Polar angle

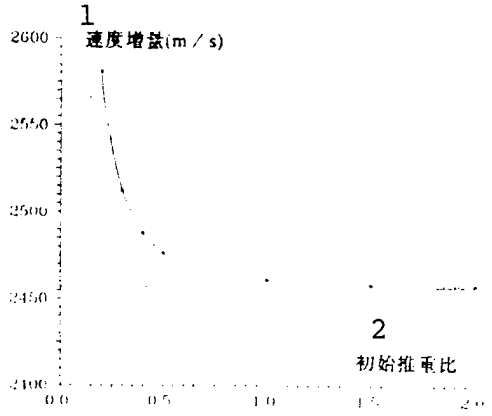

Fig. 4. Relationship between Required Velocity Increment and Thrust-Weight Ratio

Key: (1) Velocity increment;
(2) Initial thrust-weight ratio

Figure 3 shows the spacecraft altitude variation law along the optimal flight track: it descends at first and then ascends to enter the target orbit; when G=0.2, the minimum altitude is 176km, and if G decreases further, the minimum altitude of the spacecraft will decrease and even intersect with the ground. In consideration of actual needs, such as the need for avoiding a dense atmosphere, it is required to restrict the minimum altitude ($r(t)>r_{min}$). This is a problem of state variable constraints along the flight track (path constraint), which is expected to be

studied further.

Figure 4 shows the relationship between the velocity increment needed for the spacecraft to enter the target orbit and the initial thrust-weight ratio. The straight line in the figure corresponds to an ideal situation of impulsive orbital insertion, while with limited thrust, ΔV is always overstated. This difference is just the velocity loss caused by gravity--the smaller the thrust, the larger the loss can be.

Sample Calculation 2 Transfer from a circular orbit (with height 200km) to an adjacent circular orbit (500km in height). V_e=2800m/s.

In launching some satellites, the launch vehicle is required to send them onto a higher orbit. In such cases, the mission undertaken by the final stage of the rocket is similar to a fixed thrust primary entry between two circular orbits. More commonly, this kind of activity can be referred to as an optimal transfer between non-intersecting orbits. This transfer, while accomplished in an impulsive mode, requires an additional transitional orbit for a secondary orbit transfer.

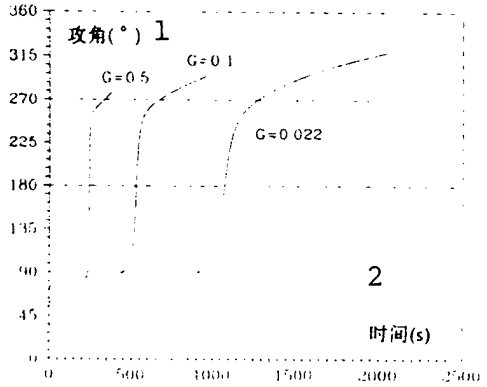

Fig. 5. Optimal Angle of Attack Variation Law
Key: (1) Angle of attack; (2) Time

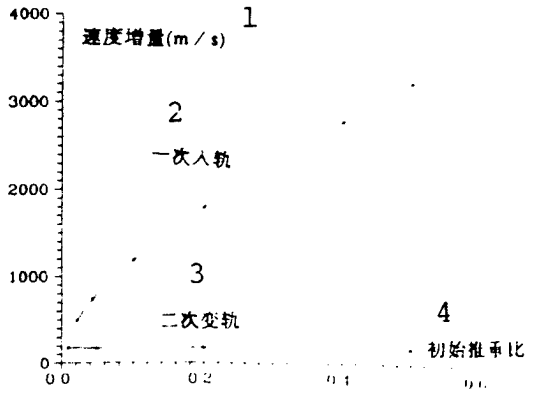

Fig. 6. Relationship between Required Velocity Increment and Thrust-Weight Ratio

Key: (1) Velocity increment; (2) Primary orbital insertion; (3) Secondary orbital transfer; (4) Initial thrust-weight ratio

Fig. 5 shows an optimal variation law of attack angle α, by which the spacecraft is flying backward during the period of time $90°<\alpha<270°$. α varies dramatically near 180° and it varies almost abruptly with a larger thrust. It can be foreseen that if α is restricted ($|\alpha(t)| \leq \alpha_{max}$), it will vary abruptly here. Fig. 6 shows the relationship between the velocity increment needed for an orbital transfer and G. During a primary orbital insertion, ΔV will increase rapidly with increase in G and therefore, a small thrust propulsion is suitable for this occasion. For comparison, a transitional orbit (h_a is 500km, h_p is 200km, ω is 180°) is utilized for studying the secondary optimal orbital transfer, for which a velocity increment must be greatly reduced as seen in Fig. 6.

5. Conclusions

(1) The thrust cannot be understated in the transfer from a parking orbit to a synchronous transfer orbit so as to avoid an overstated velocity loss. If a small thrust is to be adopted, a

more complex control program is required;

(2) During a transfer between non-intersecting orbits, a small thrust propulsion is preferable for a primary orbital insertion so as to avoid too much velocity loss. In this case, a secondary or multiple orbital transfer is generally adopted.

References

1 王小军，吴德隆. 通用灵活的顶级运载器研究. 导弹与航天运载技术，1993，(5).

2 Haissig C M, Mease K D. Minimum—fuel Power—limited Transfers Between Coplanar Elliptical Orbits. Acta Astronautica, 1993,29(1).

3 王明春，荆武兴，杨涤，吴瑶华. 能量最省有限推力同平面轨道转移. 宇航学报，1992，(3).

4 海宁吐尔，欧天垣，曹叔维译. 最优化方法. 机械工业出版社，1982.

5 院春荣著，茅振东译. 大气中飞行的最优轨迹. 宇航出版社，1987.

6 程国采. 弹道导弹制导方法与最优控制. 国防科大出版社，1987.

7 赵汉元. 再入飞行器机动弹道的设计. 宇航学报，1985，(1).

8 余梦伦. 地球同步卫星发射轨道的设计，中国空间科学技术，1993(2).

Measurement of Spacecraft Position and Attitude in Rendezvous Docking Using Computer Vision

Chai Xiping, Dai Yongjiang, Zhao Yuan, Wang Yan

(Department of Applied Physics, Heilongjiang Engineering University, Harbin, 150002)

Abstract: This paper introduces a method of measuring spacecraft position and attitude in rendezvous docking. With small computation load, this simple method can provide, through measurement, the position and attitude angle of a tracking aircraft relative to a target aircraft.

Key words: computer vision, rendezvous docking, relative position, attitude angle

1. Principle of Measurement

To successfully accomplish a rendezvous docking, it is necessary to determine the position and attitude of one aircraft relative to the other.

In 1981, an American named Fukui proposed a method of measuring robot position and attitude using computer vision technology in solving the robot navigation problem [2]. He adopted a standard rhombic pattern as shown in Fig. 1. Based on this concept, a new method and related auxiliary docking equipment used to measure the relative position and attitude angle between two aircraft are described in this paper.

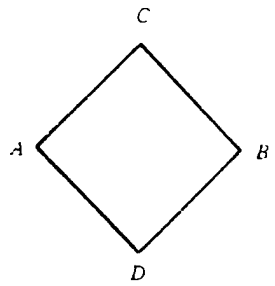

Fig. 1. Standard Pattern Used by Fukui

The auxiliary docking equipment shown in Fig. 2 is made of four semiconductor lasers arranged in the form of a square, where a three-dimensional coordinate system takes the center of the square as its original point and two diagonal lines respectively as Y and Z axes, and a line perpendicular to this plane and pointing to a camera as X axis.

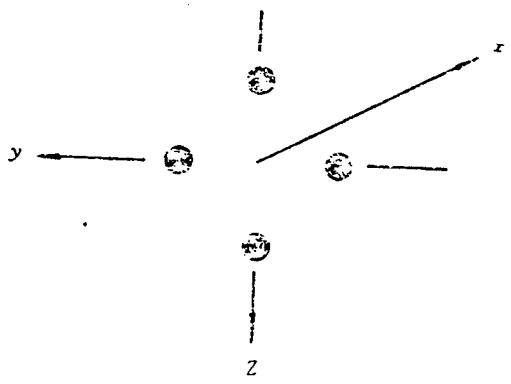

Fig. 2. Auxiliary Docking Equipment
and Docking Coordinate System

In this coordinate system, two planes, P_1 and P_2 are defined: one plane passes through two points C and D and the center of the camera, while the other passes through two points A and B and the center of the camera as shown in Fig. 3. In this way, a complex three-dimensional problem can be transformed into a simple two-dimensional problem. Two visual angles are defined: one is ψ, a tension angle of CD to CCD center, while the other is

θ, another tension angle of AB to L as shown in Fig. 4. In addition, two polar angles are also defined: one is ρ,β,ρ, an included angle between the vertical line AB that passes through the original coordinate point and the radius vector R, while the other is β, an included angle between the vertical line CD that passes through the original coordinate angle and the radius vector R as shown in Fig. 3. Thus, the planes P_1 and P_2 respectively contain a polar angle and a visual angle. Suppose the projections of C and D on CCD are C′ and D′, then the included angle between LC′ and LD′ is also ψ. Thus, ψ can be calculated based on simple geometric relations. Similarly, θ can also be calculated.

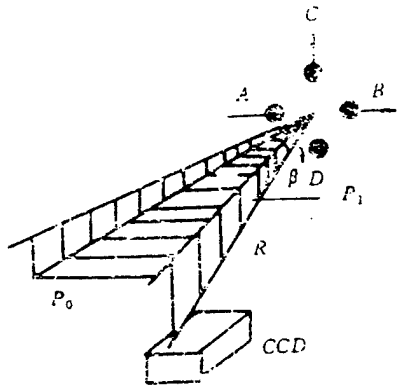

Fig. 3. Transformation of Three-dimensional Problem to Two-dimensional Problem

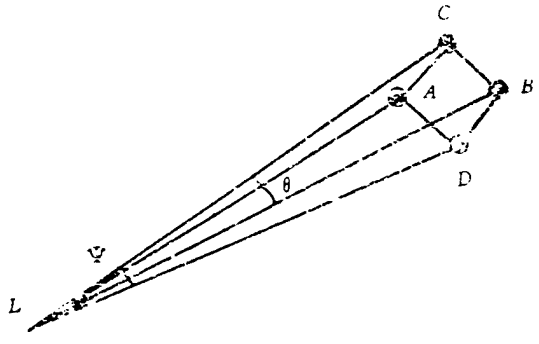

Fig. 4. Visual Angles Defined

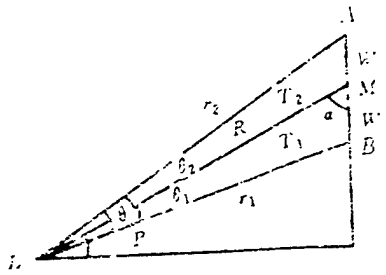

Fig. 5. Two-dimensional Geometric Relations in Plane P_2

The geometric relations in plane P_2 are shown in Fig. 5.

The radius vector R divides ΔABL into two triangles T_1 and T_2, in which

$$r_1^2 + r_2^2 = 2(R^2 + W'^2) \tag{1}$$

$$\sin\alpha = \frac{r_1 r_2 \sin\theta}{2RW} \tag{2}$$

The area of ΔABL is the sum of T_1 and T_2 areas:

$$r_1 r_2 \sin\theta = r_1 R \sin\theta_1 + r_2 R \sin\theta_2 \tag{3}$$

and

$$(2W)^2 = r_1^2 + r_2^2 + 2r_1 r_2 \cos\theta \tag{4}$$

By solving the above four equations,

$$\cos\rho = \frac{(R^2 - W^2)\mathrm{tg}\theta}{2RW} \tag{5}$$

Similarly, in P_1 plane:

$$\cos\beta = \frac{(R^2 - W^2)\mathrm{tg}\theta}{2RW} \tag{6}$$

To solve θ and ψ:

In Fig. 6, W_1 and W_2 on the image plane respectively are projections of AM and BM on the image plane. The following can be derived:

$$\mathrm{tg}\theta = \mathrm{tg}(\theta_1 + \theta_2) = \frac{f(W_1 + W_2)}{f^2 - W_1 W_2} \tag{7}$$

and ψ can be solved in the same way.

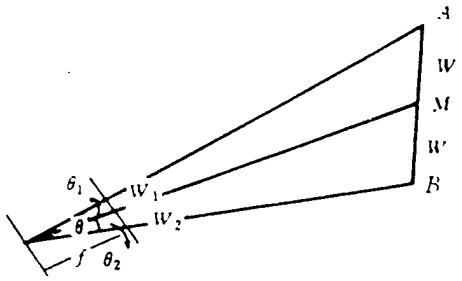

Fig. 6. Relationship Between the Projection of AB on Image Plane and θ

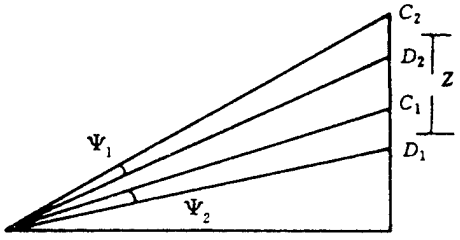

Fig. 7. Relationship between Two Patterns

2. Equation Solution

When θ and ψ are solved, there are still three unknown quantities in Eqs. (5) and (6), namely ρ, β and R. Even if R is known, β and ρ still may have double solutions, one positive and one negative, which depends on whether CCD is located to the left or right, above or below the target.

To solve the double solution problem, four more lasers of the same kind are added, which are arranged in a square form just the way they are in the auxiliary docking equipment as described above. The center of the square is positioned on Z axis at a fixed distance from the original coordinate point as shown in Fig. 7. Subsequently, the following six equations can be obtained:

$$\cos\beta_1 = \frac{(R_1^2 - W^2)\mathrm{tg}\psi_1}{2R_1W} \tag{8}$$

$$\cos\beta_2 = \frac{(R_2^2 - W^2)\mathrm{tg}\psi_2}{2R_2W} \tag{9}$$

$$\cos\rho_1 = \frac{(R_1^2 - W^2)\mathrm{tg}\theta_1}{2R_1W} \tag{10}$$

$$\cos\rho_2 = \frac{(R_2^2 - W^2)\mathrm{tg}\theta_2}{2R_2W} \tag{11}$$

$$\triangle Z = R_2\sin\beta_2 - R_1\sin\beta_1 \tag{12}$$

$$R_1\cos\beta_1 = R_2\cos\beta_2 \tag{13}$$

Here ΔZ is the distance between two squares in Fig. 7. To solve this non-linear coupled equation, six new functions $f_1, \ldots\ldots, f_6$ are defined first, which respectively are the differences between the left sides and the right sides of this coupled equation. Considering the effect of noise in practical

use, a non-linear least square method is adopted. The Jacobi matrix in the coupled equation is solved as

$$\begin{bmatrix} -\sin\beta_1 & 0 & 0 & 0 & \frac{R_1^2+W^2}{2WR_1^2}\mathrm{tg}\psi_1 & 0 \\ 0 & -\sin\beta_2 & 0 & 0 & 0 & \frac{R_2^2+W^2}{2WR_2^2}\mathrm{tg}\psi_2 \\ 0 & 0 & -\sin P_1 & 0 & \frac{R_1^2+W^2}{2WR_1^2}\mathrm{tg}\theta_1 & 0 \\ 0 & 0 & 0 & -\sin P_2 & 0 & \frac{R_2^2+W^2}{2WR_2^2}\mathrm{tg}\theta_2 \\ -R_1\cos\beta_1 & -R_2\cos\beta_2 & 0 & 0 & -\sin\beta_1 & -\sin\beta_2 \\ -R_1\sin\beta_1 & R_2\sin\beta_2 & 0 & 0 & \cos\beta_1 & -\cos\beta_2 \end{bmatrix}$$

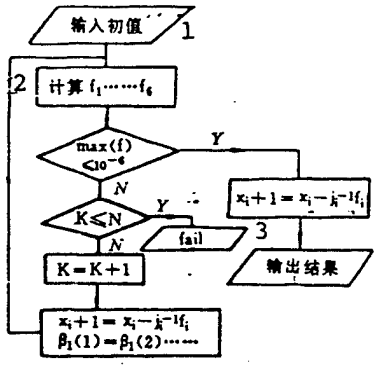

Fig. 8. Flow Chart of Computer Simulation

Key: (1) Initial input value
(2) Calculate f_1.....f_6
(3) Output result

Fig. 8 is a flow chart of computer simulation, where N is the given maximum iteration times; W, ψ_1, ψ_2, θ_1, θ_2, ΔZ are all measurable; $\beta_1(1)$, $\beta_2(1)$, $\rho_1(1)$, $\rho_2(1)$, $R_1(1)$ and $R_2(1)$ respectively are given initial values of quantities to be measured. If the maximum values of f_1,.....f_6 are smaller than or equal to 10^{-6} after iteration, then it can be believed approximately that the $\beta_1(2)$, $\beta_2(2)$, $\rho_1(2)$, $\rho_2(2)$, $R_1(2)$ and $R_2(2)$ obtained now are just β_1, ρ_1, ρ_2, R_1 and R_2 to be solved.

For instance,

Φ_1=0.0291

Φ_2=0.0314

θ_1 =0.0321

θ_2 =0.03229

W=0.1500

ΔZ=0.5000

$\beta_1(1)$=0.0785

$\beta_2(1)$=0.0785

$\rho_1(1)$=0.0785

$\rho_2(1)$=0.0785

$R_1(1)$=10.0000

$R_2(1)$=10.0000

After iteration, the final results are:

β_1=0.663

β_2=0.613

ρ_1 =0.515

ρ_2 =0.536

R_1=8.124

R_2=7.826

In fact, β_1 and ρ_1 are the pitch angle and side slip angle of the target relative to CCD, from which the relative position of the target is derived as:

$$x = R_1\cos\beta_1\cos\rho_1,$$
$$y = R_1\cos\beta_1\sin\rho_1,$$
$$z = R_1\sin\beta_1$$

3. Conclusions

This paper describes a method of measuring the position and attitude angle of two spacecraft by transforming a three-dimensional problem into a two-dimensional problem. Based on simple geometric relations, two coupled equations can be derived, which contain three unknown numbers. To solve these coupled equations, one more auxiliary docking equipment of the same kind is added. The required information about the position and attitude angle can be acquired after iteration.

This paper, a project funded by State 863 Program, was received on May 27, 1993.

References

1 Courtney J W. Robot Guidance Using Computer Vision. Pattern Recogniton, 198-, 17(6):582—592.

2 Fukui Y. TV image processing to determine the position of a robot vehicle. Pattern Recognition, 1981, 14:101—109.

3 Art J Ray. Rendezvous And Docking Tracker. AAS 86—014, 1986.